Recognizing and correcting for errors in frequency-dependent modulation spectroscopy

Wilson, N M ; Aarnio, H; Österbacka, R

Published in:
Physica Scripta

DOI:
10.1088/1402-4896/ad03bf

Published: 01/11/2023

Document Version
Accepted author manuscript

Recognizing and correcting for errors in frequency-dependent modulation spectroscopy

N M Wilson[1], H Aarnio[2] and R Österbacka[1]

[1] Physics, Faculty of Science and Engineering, Åbo Akademi University, Henriksgatan 2, 20500 Turku, Finland
[2] Mathematics and physics, Centria University of Applied Sciences, Bondegatan 2, 67100 Karleby, Finland

E-mail: Ronald.Osterbacka@abo.fi

Abstract.

This work shows how to acquire reliable data from frequency dependent continuous-wave modulation spectroscopy. We demonstrate this through the example of continuous-wave photoinduced absorption (cwPA), a characterization technique useful for studying long-lived photoexcitations in thin-film solar cell materials. Experimental errors arising at moderate frequencies in modulation spectroscopy are identified and corrected for. Limitations of the detectors and electronics are seen to cause both signal loss and phase shifts. Imperfect charge collection in the detector leads to wavelength-dependent correction factors, while phase shifts caused by the experimental setup call for frequency-dependent corrections. The methods outlined in this work act as a guide to avoid pitfalls in setting up modulation spectroscopy measurements and correcting for limitations.

Keywords: photomodulation spectroscopy, modulation spectroscopy, photoinduced absorption, continuous-wave photoinduced absorption, phase-sensitive measurements, pump-prope spectroscopy, organic semiconductors
Submitted to: *Phys. Scr.*

1. Introduction

Continuous-wave modulation spectroscopies can be used to observe reflectance and absorbance to gain insight into material properties and the dynamics of long-lived photoexcitations [1, 2, 3]. These spectroscopic techniques all use a periodically varying modulation, such as light or electric field, to probe the properties of a material while measuring a spectroscopic response. The modulation will lead to a periodicity in the measured signal. This enables the use of lock-in techniques, which have the capacity to single out minimal signals as long as they repeat at a specified frequency. Thereby we can eliminate random noise and get a very sensitive measurement. Changing the modulation frequency can be used to probe material dynamics but care must be taken when working with higher frequencies, as made evident in this work.

Continuous-wave photoinduced absorption (cwPA) is) is a measurement technique that provides information about the recombination and generation of long-lived excitations in thin films of organic semiconductors [4, 5, 6, 7]. The measurement is relatively simple to its setup and provides information about processes in the bulk of the material without being overshadowed by contact effects. The measurement only requires a film of the active material to enable characterization of the material's photophysical properties.

Here we discuss problems arising in modulation spectroscopies, exemplified by using cwPA, and provide tools for correcting them. The setup is described in section 2. Section 3 discusses handling background disturbances in the setup. In section 4 we discuss problems caused by the limitations of detectors and how these can be identified. Section 5 explores the impact of phase shifts. Lastly, section 6 demonstrates how all the previously discussed effects impact two example data sets.

2. Continuous-wave Photoinduced Absorption

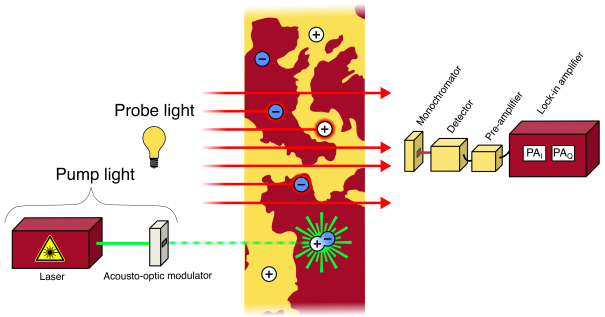

Figure 1. Schematic of the experimental cwPA setup. (Licensed as CC BY 4.0, N M Wilson (2022), https://doi.org/10.6084/m9.figshare.19086518.v1)

The cwPA setup consists of a pump light, which generates photoexcitations in the sample, and a probe light, for which the change in transmission due to the photoexcitations is measured. Figure 1 shows a sketch of the setup. The pump light is modulated through an acousto-optic modulator or mechanical chopper, and focused on the sample. In our setup a 514 nm laser beam is modulated into light with sinusoidally varying intensity. The sample is a thin film of a material, e.g., one used as the active layer in solar cells known to efficiently generate free charge carriers. The modulation function (sine wave) is controlled by a function generator. Note that throughout this article when discussing "frequency" we refer to the modulation frequency with which the pump light intensity varies.

As a probe light, we use a broad spectrum tungsten lamp with constant intensity, cut off by a long-pass filter to prevent generating unwanted background excitations in the sample. Some of this light will be absorbed by the sample, while the transmitted part will be guided into a monochromator and collected by a detector. The detected signal goes via a pre-amplifier to a lock-in amplifier (Stanford Research Systems SR830 DSP), which analyzes the signal in relation to the modulation frequency. The lock-in amplifier only records the components of the signal that have the same frequency as the modulation. This means that the lock-in amplifier only measures the transmission change caused by the pump light (ΔT). The results are given as in-phase, which has the same frequency and phase as the pump, and quadrature, which has the same frequency but is phase-shifted by $\pi/2$. For example, if the pump varies as $\sin \omega t$ the in-phase will be the amplitude of the $\sin \omega t$-component when the transmission is analyzed as a Fourier series. Similarly, the quadrature is the amplitude of the $\cos \omega t$-component.

There will always be phase shifts in the setup in actual measurements, which must be considered to determine the true in-phase and quadrature. The initially recorded data will be two values, phase 1 and phase 2, phase-shifted with respect to each other by $\pi/2$. Obtaining in-phase and quadrature from these is not always trivial, which is discussed in Section 5.

By blocking the probe light and repeating the measurement, we obtain the lu-

minescence signal, which is subtracted from the transmission values to determine the actual change ΔT. Finally, the transmission change is normalized to the transmission without the influence of the pump light (T) to cancel effects from the setup geometry, detector efficiencies and optical losses. To measure T with the lock-in amplifier a modulation is temporarily applied to the probe light, using a mechanical chopper.

For a thin film the normalized change in transmission due to the photogenerated excitations ($-\Delta T/T$) is directly proportional to the density (n) of long-lived excitations absorbing at that particular probe wavelength. Using this, photoinduced absorption is defined as [3]

$$PA = -\frac{\Delta T}{T} = n\sigma d, \tag{1}$$

where σ is the absorption cross-section and d is the film thickness. Instead of working with the in-phase (PA_{I}) and quadrature (PA_{Q}) component of $-\Delta T/T$, we often look at the radius signal $PA_{\mathrm{R}} = \sqrt{PA_{\mathrm{I}}^2 + PA_{\mathrm{Q}}^2}$. The radius can be calculated from any two components shifted with $\pi/2$ to each other, meaning we can use the two raw components from the measurement, phase 1 and phase 2. The radius can sometimes be a more reliable source of information than PA_{I} and PA_{Q} as it is not affected by errors in the phase. However, if the phase can be reliably determined, PA_{I} and PA_{Q} contain more information and give the benefit of extracting parameters from fitting two curves instead of one.

One way to gain information about the photoexcitation dynamics from PA_{R} is to look at its frequency dependence, typically plotted on a log-log scale. When approaching low frequencies the curve saturates to a value of $G\tau\sigma d$, where G is the generation rate, τ is the lifetime of the photoexcitations, σ is the cross-section and d is the thickness of the film [4, 8]. Around the point defined by $\omega\tau = 1$ the curve starts to drop, until it reaches a linear slope, ideally of ω^{-1}. For some materials the slope can be less steep, but still close to ω^{-1} [7, 9]. This is assigned to dispersive phenomena originating in relaxation processes. At high enough frequencies, the value of PA_{R} will be directly proportional to the generation and independent of the lifetime (for non-dispersive materials). The behavior is the same regardless of the waveform of the modulation. In section 6 we illustrate how different experimental errors impact this part of an $PA(\omega)$-plot. If we instead wish to study recombination we can use square wave modulation and look at the low-frequency quadrature to access the reaction order or the intensity dependence to access the bimolecular recombination constant [7, 8].

3. Background disturbance

Using a lock-in amplifier to isolate a specific frequency effectively minimizes noise, as noise with any other frequency than the modulation will be eliminated. Nonetheless, the risks of picking up background interference need to be addressed. When measuring the luminescence we observe a small but distinguishable frequency-dependent signal that becomes more prominent as the frequency increases. This signal remains when repeating the exact measurement with the pump light turned off in our setup. Therefore we conclude that this is not luminescence or any other optical signal, but some interference originating internally in the setup. This signal has a clear frequency dependence, as illustrated in figure 2. Here we plot the two raw phases phase 1 and phase 2. As the signal does not seem to depend on the detector, we use one polynomial fit for all curves.

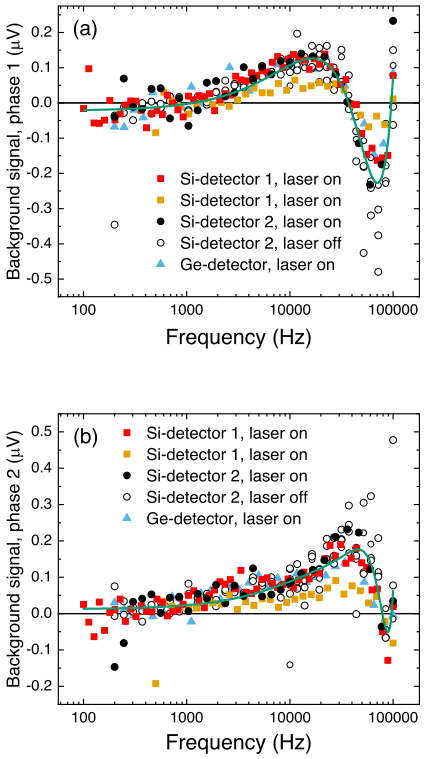

Figure 2. Background signal separated into the two raw phases. Data for two silicon detectors and a germanium detector. One dataset was recorded without the laser turned on, revealing that this is not luminescence. The solid line is a polynomial fit to all data points.

4. Detector response

All detectors are limited by the time it takes to react to an incoming signal. This can lead to a loss of amplitude for a modulated signal, as the rise and decay times make peaks and valleys less sharp. As the lock-in amplifier gives values proportional to the amplitude this causes signal loss. An example is illustrated in figure 3. The figure also shows the phase shift caused by the detector, discussed in section 5.

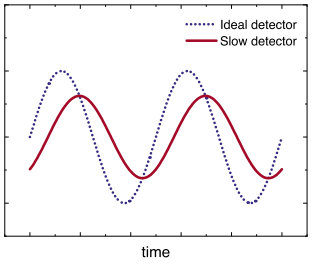

Figure 3. Illustration of how a sinusoidal signal is distorted by a slow detector response. The dotted line shows a perfect, infinitely fast response and the solid line shows how the signal can be modified by a slow detector.

Here we look at two silicon detectors, which we call detector 1 and detector 2. Detector 1 is a silicon photodiode (model AR-989A) by AME AS, specified to have a rise time of 16 ns and an area of 33 mm^2. The second photodiode, detector 2 is model UV-50 by UDT Sensors Inc., with a rise time of 3.5 μs at 254 nm and an area of 50 mm^2. We characterize the response times of the detectors by measuring their response to diode lasers of different wavelengths, with built-in modulation forming a square wave. As seen by the lock-in amplifier, the loss of radius signal (amplitude) at the different wavelengths can be seen in figure 4. Both detectors display a decrease at higher frequencies but with different wavelength dependencies. Detector 1 shows a drastic decrease in signal amplitude at longer wavelengths, while the response of detector 2 remains almost unchanged. The shape of these curves is linear in intensity over several orders of magnitudes, as shown in the supplementary material, figure S1. The wavelength-dependent behavior is probably caused by longer wavelengths penetrating deeper into the detector. This can lead to carrier generation outside the depletion region, meaning there will be slow charge collection as carriers first need to be transported by diffusion [10]. Following the same logic, the lack of wavelength dependence of detector 2 can be explained by a wider depletion region. The slow response of detector 2 at all wavelengths could indicate a smaller electric field than that in the depletion region in detector 1.

Figure 5 shows the response of the two detecors to the diode lasers as measured in an oscilloscope. For detector 1 we clearly see how the shorter wavelengths are closer to a square wave while the longer wavelengths are more deformed and have a smaller amplitude. The data for 730 nm deviates clearly and shows a substantial overshoot. This is an artifact arising from an overshoot in the modulation shape created by the diode laser and is not an effect of the detector. As expected detector 2 displays a much weaker wavelength dependence but a more substantial deviation from a square

wave.

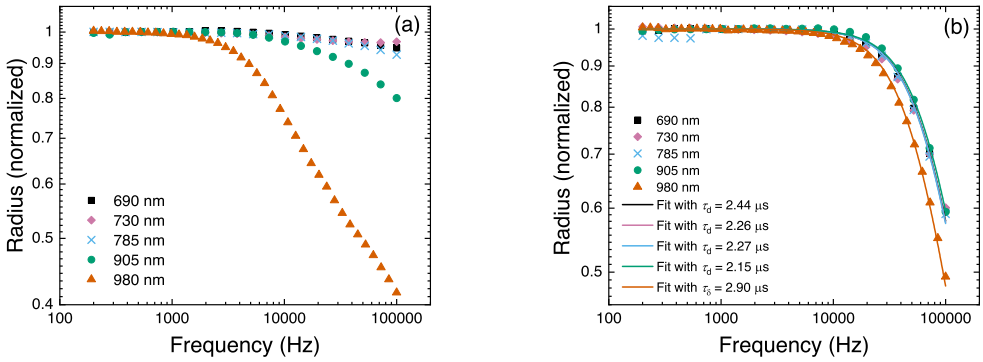

Figure 4. Response of silicon detectors to square wave modulated laser diodes with different wavelengths. The radius as recorded by the lock-in amplifier for detector 1 (a) and detector 2 (b). Response for detector 2 fitted with (3).

Ideally, we would have a detector that is so fast that these problems do not occur, but the second-best option is to correct it afterwards, given that we can calibrate for the frequency response of the detector. A detector such as detector 1 will give reliable results at short wavelengths, whereas correcting at longer wavelengths requires calibration measurements close to the wavelength at which we want to study the photoexcitations. On the other hand, a detector such as detector 2 will need to be corrected at a wide range of wavelengths, but the same calibration curve can be used for a large part of this spectrum.

For this kind of correction to be possible, the detector's response can not be dependent on the shape of the incoming signal. Otherwise, we could get a situation where we use a particular shape to determine the correction factor, but the actual shape from ΔT acts differently. As the lock-in amplifier only measures first harmonic components, we need the first harmonic components coming into the detector to give first harmonics coming out. This means that none of the information is lost. This will indeed be the case as delaying a sinusoidal signal will never cause a change in its frequency, only phase (a longer argument for this can be found in the supplementary material).

As the percentual loss of the radius signal depends neither on intensity (figure S1) nor modulation shape we can use it as a correction factor to ascertain the actual ΔT values. If we assume that the signal decay of the detector has an exponential form we can calculate the mathematical form of the loss. The calculations can be found in the supplementary material, and give the signal amplitude at time t from an sine-shaped input as

$$A(t) = R_0/2 \left(\frac{-1(\omega\tau_\mathrm{d} \cos \omega t - \sin \omega t)}{(\omega\tau_\mathrm{d})^2 + 1} + 1 \right). \tag{2}$$

Here the time τ_d describes the electrical response of the detector and R_0 is the peak generation rate. Looking solely at the time-dependent parts gives a signal described

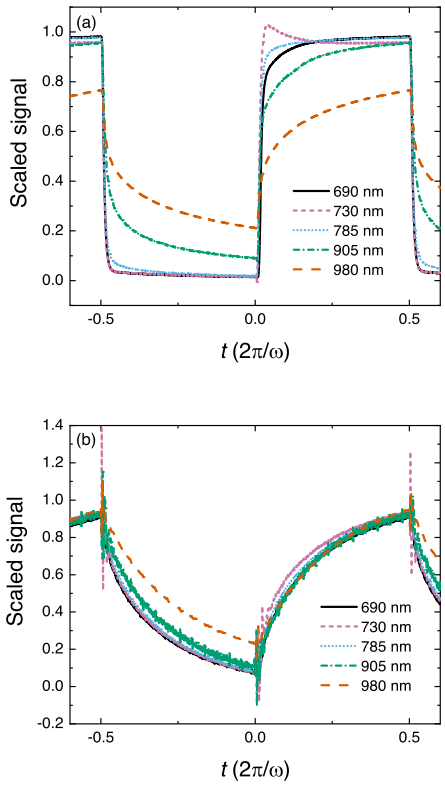

Figure 5. Response of silicon detectors to square wave modulated laser diodes with different wavelengths. The signal as recorded by oscilloscope for detector 1 (a) and detector 2 (b) at 100 000 Hz. The scale equates 0 and 1 with the square wave response at a low frequency, where the detector response is sufficiently fast.

by $\omega\tau_\mathrm{d}\cos\omega t - \sin\omega t$. The radius will be proportional to

$$\frac{N_0\sqrt{(\omega\tau_\mathrm{d})^2+1}}{(\omega\tau_\mathrm{d})^2+1} = \frac{N_0}{\sqrt{(\omega\tau_\mathrm{d})^2+1}}. \tag{3}$$

Fitting the radius as a function of frequency with (3) gives excellent agreement for detector 2, as seen in figure 4b. A combined fit to all the curves gives a value of τ_d =2.4 μs (figure S2), while individual fits range between 2.15 and 2.90 μs, with 980 nm giving a somewhat longer τ_d than the others. For detector 1 a reasonable fit is impossible, as the dynamics involving diffusion outside the depletion layer can not be captured in a simple exponential.

5. Phase shift

The lock-in amplifier will compare the signal from the detector with a specific frequency and phase. The function generator uses these same parameters to create a sine wave sent as a reference to the acousto-optic modulator. This ensures that we measure the transmission change only at the chosen frequency. However, there will be some shifts in timing as the sine wave passes through the setup. Firstly, there might be a constant phase shift θ_0 between the signal from the lock-in amplifier and the sine wave realized by the acoustic-optic modulator. This arises when signal is conveyed from the lock-in amplifier to the function generator, and from the function generator to acousto-optic modulator. It depends on the triggering method and how each piece of equipment contructs the signal that is conveyed to the next step. Secondly, we can expect a frequency-independent time delay δt due to delays in the measurement setup electronics. This will shift a pure sine wave to $\sin\omega(t-\delta t)$. Thirdly, the distortion of the signal caused by a slow photodetector will also delay the timing of the wave. This can be seen in equation 2 and figure 3, where detector 2 has shifted $\sin\omega t$ to $\omega\tau_\mathrm{d}\cos\omega t - \sin\omega t$. All these phase shifts can be corrected for in measurement data as long as we have a good mathematical description of them.

The phase describes the timing of a periodic signal and is defined as $\arctan(Q/I)$, where I and Q are the in-phase and quadrature signal, respectively. For the signal distorted by the detector, the phase becomes $-\arctan\omega\tau_\mathrm{d}$ (as the sine component here forms the in-phase). The total phase shift describing the difference in timing between a peak in the sinusoidal signal used as reference by the lock-in amplifier and the signal going into the lock-in amplifier from the photodetector will thus for detector 2 be $\theta_0 - \omega\delta t - \arctan\omega\tau_\mathrm{d}$. For detector 1 we do not have an analytical approximation and thus no calculated phase shift.

We need to know all phase shifts to separate the PA-signal into quadrature and in-phase reliably. When the frequency is low compared to the detector response, i.e., $\omega\tau_\mathrm{d} \ll 1$ and $\arctan\omega\tau_\mathrm{d} \approx \omega\tau_\mathrm{d}$, the phase shift for detector 2 will be $\theta_0 - \omega\delta t - \omega\tau_\mathrm{d}$. This linear frequency dependence is confirmed in figure 6. Here we have measured the pump light at 514 nm modulated to a sine wave (without any probe light) and calculated the phase. As we do not know the true in-phase, the phase is given in relation to phase 1. In an ideal situation, the phase would be constant regardless of frequency. The linear slope corresponds to $\delta t + \tau_\mathrm{d} = 3.9$ μs. Subtracting $\tau_\mathrm{d} = 2.4$ μs from the fit in figure 4 gives $\delta t = 1.5$ μs. This is the delay caused by electronics in the setup. The intercept at $\omega = 0$ corresponds to a constant phase shift $\theta_0 = 0.33$.

When all parameters governing the phase shift are known we can correct the data. To do this we calculate the phase of the signal (as PA_1 and PA_2) and subtract the phase shift $\theta_0 - \omega\delta t - \arctan\omega\tau_\mathrm{d}$, resulting in a corrected phase θ. The signals are then calculated as $PA_\mathrm{I} = -PA_\mathrm{R}\cos(\theta)$ and $PA_\mathrm{Q} = PA_\mathrm{R}\sin(\theta)$.

For detector 1 the same procedure is not possible, as we do not have a function that fits the signal radius loss. We conclude that for detector 1 we can not draw any reliable conclusions about the phase, and therefore phase separated data is unattainable at higher frequencies. However, PA_R is not affected by phase shifts and can still be analyzed.

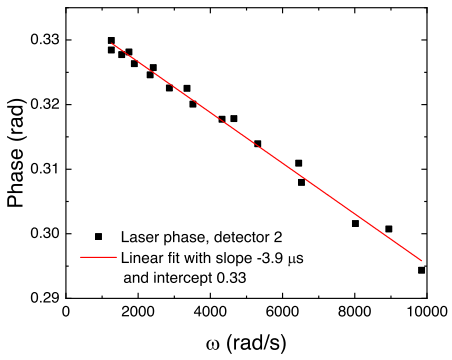

Figure 6. Phase shift of modulated pump light measured with detector 2 at $f < 10000$ Hz.

6. Impact on cwPA results

We have discussed several factors that introduce problems during the measurement. Here we will demonstrate how to correct for these in two actual datasets, acquired from performing cwPA on polymer:fullerene blends. Analysis of the corrected datasets is published concurrently in [11]. The first example is measured at 985 nm on a 1:1 blend of P3HT:ICBA (poly(3-hexylthiophene): indene-C60 bisadduct) with detector 1 and the second is measured with detector 2 at 1050 nm on a film of PTB7:PCBM (Poly[[4,8-bis[(2-ethylhexyl)oxy]benzo[1,2-b:4,5-b']dithiophene-2,6-diyl][3-fluoro-2-[(2-ethylhexyl)carbonyl]thieno[3,4-b]thiophenediyl]] :[6,6]-phenyl-C61-butyric acid methyl ester) in a 1:1 blend (with DIO). In figure 7a-b we see the raw PA data, divided into phase 1 and phase 2. The solid line marks the background signal for the two phases. PA_{R} is calculated after subtracting this background, resulting in the data in figure 7c-d. These are then corrected for the percentual detector loss of the same form as shown in figure 4. For detector 2 we use a fit of the loss at 980 nm with (3), seen in figure 4 and giving $\tau_{\mathrm{d}} = 2.90\ \mu s$. Correcting a measurement at 1050 nm without calibration data exceeding 980 nm is not ideal, as we can not confirm if the detector develops a wavelength dependence above 980 nm. We use it here for illustrative purposes to correct this dataset, measured before the detector limitations were discovered. For detector 1 we fit the response at 980 nm with a piecewise function of three lines linear in the log-log plot. The corrections change the PA_{R} values more at higher frequencies, which is the regime that can be used to determine the generation rate G. Do note how, in both cases, the slope changes from an unphysical slope < -1 to a less steep one. Without this correction $PA_{\mathrm{R}}(\omega)$ fits are impossible as the underlying theory does not allow such slopes. It can also be seen how subtracting the background gives a smoother and more linear slope. For detector 2 we can use the phase shift discussed above and correct PA_1 and PA_2 to PA_{I} and PA_{Q}.

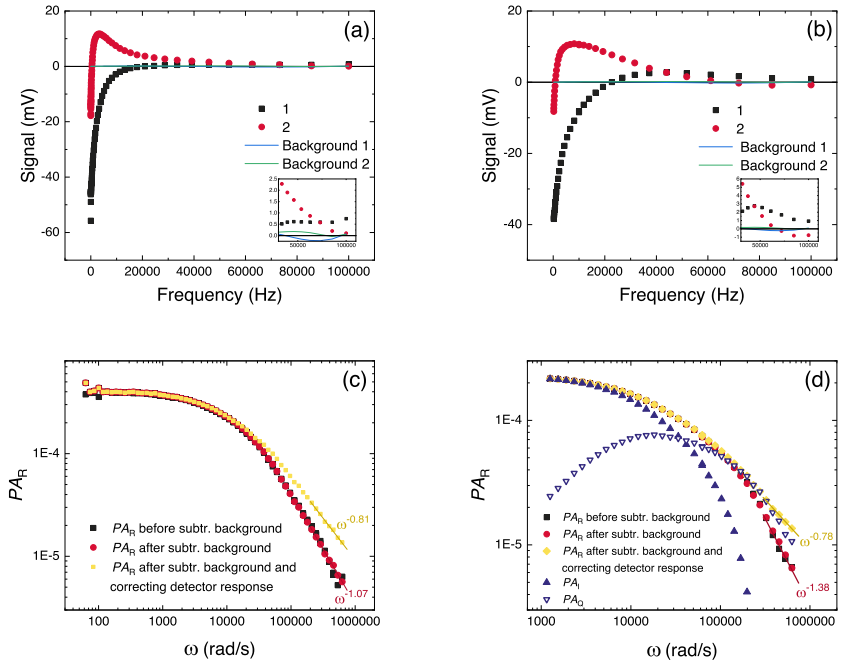

Figure 7. Example of how the corrections impact two datasets when measuring cwPA. The raw datasets (ΔT) and background disturbance, for (a) P3HT:ICBA measured with detector 1 (T = 140 K, λ = 985 nm) and (b) PT7B:PCBM measured with detector 2 (T = 90 K, λ = 1050 nm). The inset shows the same data at high frequencies, where the background is the largest. Calculated PA_R before and after subtracting the background disturbance for the same datasets, detector 1 in (c) and detector 2 in (d). For detector 2 PA_I and PA_Q, resulting from phase correcting PA_1 and PA_2, is shown. For both detectors the impact of correcting for signal loss due to the detector response is shown.

7. Conclusions

Frequency-dependent modulation spectroscopy offers valuable tools for material characterization. We have used cwPA as an example to demonstrate how to achieve reliable results, even at high frequencies. The most significant source of error is the photodetector, and users must be aware of the limitations of the specific detector in their lab. Changes in the frequency response at long wavelengths are important to identify. Ideally, the user has access to a detector with high enough speed and sensitivity at the desired wavelength, but we show how the detector's limitations can be corrected for afterwards. We also emphasize the importance of handling phase shifts with care, as they have many components, some of which are frequency and wavelength-dependent.

Acknowledgments

Personal grants from Otto A. Malm foundation, Alfred Kordelin Foundation, Fortum and Neste Foundation and The Swedish Cultural Foundation in Finland are

acknowledged by N.M.W.

References

[1] Cardona M 1970 *Modulation Spectroscopy of Semiconductors* (Braunschweig: Friedr. Vieweg + Sohn GmbH, Verlag) URL http://dx.doi.org/10.1016/B978-1-4831-2427-8.50007-3
[2] Pollak F H and Shen H 1993 *Materials Science and Engineering* **R10** 275–374 URL https://doi.org/10.1016/0927-796X(93)90004-M
[3] Brabec C J and Dyakonov V 2003 Photoinduced charge transfer in bulk heterojunction composites *Organic Photovoltaics, Concepts and Realization* ed Brabec C J, Dyakonov V, Parisi J and Sariciftci N S (Berlin, Heidelberg, Berlin: Springer) chap 1, pp 1–56
[4] 1993 *Physical Review B* **48** URL https://doi.org/10.1103/PhysRevB.48.14809
[5] Dellepiane G, Cuniberti C, Comoretto D, Musso G F, Figari G, Piaggi A and Borghesi A 1993 *Physical Review B* **48** 7850–7856 URL https://doi.org/10.1103/PhysRevB.48.7850
[6] Wohlgenannt M, Graupner W, Leising G and Vardeny Z V 1999 *Physical Review B* **60** 5321–5330 URL https://doi.org/10.1103/PhysRevB.60.5321
[7] Westerling M, Vijila C, Österbacka R and Stubb H 2004 *Physical Review B* **69** 1–8 ISSN 01631829 URL https://doi.org/10.1103/PhysRevB.69.245201
[8] Wilson N M, Sandén S, Sandberg O J and Österbacka R 2017 *Journal of Applied Physics* **121** ISSN 10897550 URL https://doi.org/10.1063/1.4977505
[9] 2001 *Physical Review B* **63** ISSN 0163-1829 URL https://doi.org/10.1103/PhysRevB.63.125206
[10] Hamamatsu 2022 *Technical note: Si photodiodes* Solid state division, Hamamatsu Photonics K.K Ichino-cho, Higashi-ku, Hamamatsu City, Japan
[11] Wilson N M, Aarnio H and Österbacka R Submitted concurrently with this article